energies

MDPI

Article

Minimum Set of Rotor Parameters for Synchronous Reluctance Machine and Improved Optimization Convergence via Forced Rotor Barrier Feasibility †

Branko Ban [1], Stjepan Stipetic [1,*] and Tino Jercic [2]

[1] Faculty of Electrical Engineering and Computing (FER), Department of Electric Machines, Drives and Automation, University of Zagreb, Unska 3, 10000 Zagreb, Croatia; branko.ban@fer.hr
[2] Cognitio Elektronika, Bani ul. 73A, 10010 Zagreb, Croatia; tino@cognitio-elektronika.hr
* Correspondence:: stjepan.stipetic@fer.hr
† This paper is an extended version of our paper "Design and Optimization of Synchronous Reluctance Machine for actuation of Electric Multi-purpose Vehicle Power Take-Off" published in 2020 International Conference on Electrical Machines (ICEM).

Abstract: Although rare earth materials are the critical component in high torque density permanent magnet machines, their use has historically been a commercial risk. The alternatives that have been in the recent industry focus are synchronous reluctance machines (SyRM). They have lower torque density but also relatively low material cost and higher overload capability. Multi-layer IPM and SyRM machines have significant geometric complexity, resulting in a high number of parameters. Considering that modern machine design requires the use of optimization algorithms with computational load proportional to the number of parameters, the whole design process can take several days. This paper presents novel SyRM parameterization with reduced number of parameters. Furthermore, the paper introduces the novel forced feasibility concept, applied on rotor barrier parameters, resulting in improved optimization convergence with overall optimization time reduced by 12.3%. Proposed approaches were demonstrated using optimization procedure based on the existing differential evolution algorithm (DE) framework.

Keywords: electric machine; synchronous reluctance; optimization; comparison; differential-evolution; design; electric; rare-earth free; forced feasibility

Citation: Ban, B.; Stipetic, S.; Jercic, T. Minimum Set of Rotor Parameters for Synchronous Reluctance Machine and Improved Optimization Convergence via Forced Rotor Barrier Feasibility. *Energies* **2021**, *14*, 2744. https://doi.org/10.3390/en14102744

Academic Editor: Chunhua Liu

Received: 6 April 2021
Accepted: 6 May 2021
Published: 11 May 2021

1. Introduction

To reduce environmental impact, global legislation is pushing to increase electric vehicle (EV) production [1]. In addition to regulatory requirements, consumers are demanding cleaner and safer vehicles. This has led to a tectonic shift in the automotive industry, both in terms of knowledge and production, forcing the industry to evolve rapidly.

At the moment, passenger vehicles are leading the market development (Tesla, Toyota, BMW), mainly because of lighter vehicles that require smaller traction batteries. On the other hand, commercial vehicles are much heavier and require large battery capacity, resulting in significant production costs. Therefore, the commercial vehicle industry is forced to move into niche markets, such as medium-duty, short-haul, and last mile applications. Long-haul vehicle development is likely to take more time and have even more sensitive financing.

Examples of commercial vehicles suitable for SyRM adoption include electric multi-purpose vehicles (eMPVs), such as refuse trucks, hook loader trucks, or vacuum trucks [2]. eMPVs must actuate additional body systems (usually through some type of hydraulic pump) in addition to electric propulsion. Traditionally, this actuation is done by a diesel engine or a gearbox-mounted output shaft referred to as power take-off (PTO). Considering price, overload capability, and production simplicity, SyRM can be a viable ePTO solution [2,3].

This paper presents novel SyRM parameterization with a reduced number of parameters (rotor nomenclature according to Figure 1). During the optimization process, infeasible models may occur. Depending on the designer's choice, the infeasible models can be rejected or modified until they become feasible. The idea is that the procedure does not discard randomly generated infeasible geometry but modifies it until feasibility is achieved (hence the name "forced" feasibility).

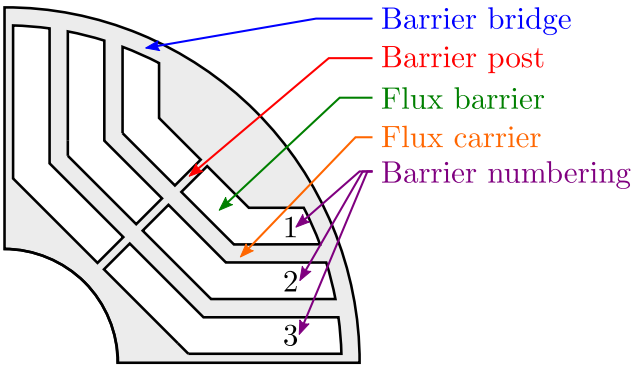

Figure 1. SyRM rotor nomenclature [3].

2. SyRM Design

2.1. Peak Performance Requirements

The machine requirements in this paper are derived from Reference [3]. All peak performance requirements are listed in Table 1.

Table 1. Peak operation requirements at base speed.

Description	Symbol	Value	Unit
Base speed	n_b	1700	rpm
Max. operating speed	$n_{\max}$	2500	rpm
Max. over speed	$1.2 \cdot n_{\max}$	3000	rpm
Max. torque	$T_{\max}$	600	Nm
Battery voltage	U_{DC}	610	V
Max. phase current	$I_{s\,\max}$	310	A_{rms}
RMS current density	J	18.4	A/mm^2

2.2. Optimization Method

Most of the requirements for the design of electrical machines are in conflict with each other (reduction of volume or mass, increase of efficiency, etc.). This is evident in the problem of increasing efficiency [4–6] through global legislative initiatives [1]. For traction drives, high efficiency in limited packaging space is an absolute imperative [7]. Therefore, a manual design that satisfies all constraints can be an overwhelming task due to a large number of coupled parameters that affect the performance and quality of the machine.

According to Pellegrino [8,9], the computational load increases proportionally with the number of geometric parameters. This is inherently the case for IPM and SyRM machines, leading to a high number of optimization variables and a longer optimization time.

Today, optimization algorithms enjoy great popularity among designers of electrical machines [10–16]. The personal experience of the designer should not be underestimated, but, due to the non-linearity and complexity of the relationships between the geometry of electrical machines and their performance, it is generally believed that only mathematical optimization can push the boundaries to better designs.

Optimization algorithms can be divided to gradient based methods and stochastic or metaheuristic methods (PyOpt provides several open-source algorithms [17]). Gradient type methods converge fast but have difficulties with global optima. Usually they require feasible starting point which can be a problematic task in complex problems (Quasi Newton method [18]). Stochastic methods are heavily used in electrical machine optimization (Pow-

ell's method [18], Nelder-Mead method [19]). The disadvantage is that the convergence can last for days, and global optimum cannot be mathematically proven. On the other hand, from engineer's point of view, these methods can find a satisfying global result. Popular metaheuristic methods are based on natural behavior (Evolutionary algorithm [20], Differential evolution [21], Particle Swarm [22]).

All methods are generally set to solve a single or multi-objective problem. The goal of design optimization is to have a chosen objective function $f(\vec{x})$ reach its minimum or maximum value while keeping other engineering indices within an acceptable range [23].

The use of finite element analysis (FEA) is inevitable in the case of SyRM's because saturation in the rotor bridges and posts significantly affects the final performance. FEA is computationally intensive and optimization can require thousands of calculations trough generations. Significant time savings can be achieved if all calculations are performed using magnetostatic simulations with fixed rotor position. Detailed explanation of different approaches for calculation of IPM machine parameters and performance using only magnetostatic simulations is available in Reference [24].

This paper uses an improved version of DE algorithm proposed by Žarko et al. [25] based on Lampinen's constraint function approach [21,26,27].

2.3. Preset Model

The number of slots and poles is chosen to be 36/4 with 4 rotor flux barriers, resulting in a two-layer integer slot winding with distributed overlapping coils. This combination provides a good compromise between the inherent ability to mitigate torque pulsations, susceptibility to noise, and the ability to use multiple parallel paths.

The ideal number of turns per coil (N_c) and parallel paths (a_p) for matching the base speed is automatically calculated based on winding feasibility [28] and ultra-fast scaling laws [29].

The goal of this paper is to prove that the forced feasibility approach (which will be discussed in later sections) yields a shorter optimization time. Considering that the selected machine has a relatively large number of parameters, all non-rotor parameters are taken from the optimized machine design in Reference [3] (Table 2). In addition, the initial design is constrained by peak performance requirements at the base speed (Table 1).

A set of parameters which are subject to optimization are listed in Table 3; colors and numbering in Tables 2 and 3 correspond to Figure 2.

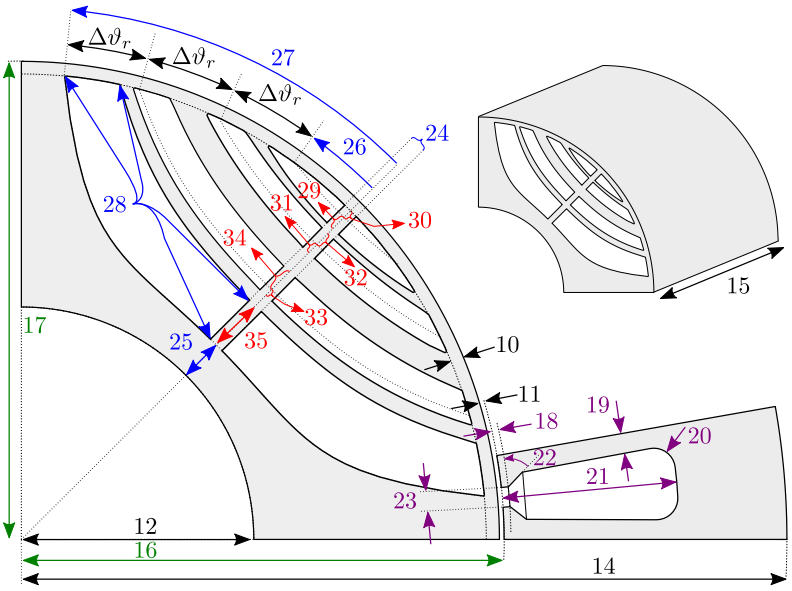

Figure 2. List of parametrization variables.

Table 2. Constant parameters.

No:	Symbol	Description	Value	Unit
1	D_s	Stator diameter	240	mm
2	D_{sh}	Shaft diameter	65	mm
3	N_{ph}	Phase number	3	-
4	N_c	No. of turns	Auto calculated	-
5	a_p	Parallel paths	Auto calculated	-
6	y_c	Coil pitch	6	-
7	N_{bar}	Barrier number	4	-
8	p	Pole pairs	2	-
9	N_s	Slot number	36	-
10	w_{bb}	Barrier bridge	0.500	mm
11	δ	Airgap	0.650	mm
12	$D_{\text{sh}}/2$	Shaft radius	32.500	mm
13	$\Delta r_{4\text{ in}}$	Barrier offset	0	mm
14	$D_s/2$	Stator radius	120	mm
15	$l_{\text{s max}}$	Active length	344.141	mm
16	D_b	Stator bore	136.751	mm
17	$\frac{D_b-2\delta}{2}$	Rotor radius	67.725	mm
18	d_t	Tooth tip depth	0.857	mm
19	w_t	Tooth width	6.874	mm
20	r_{sc}	Slot corner rad.	1.588	mm
21	d_s	Slot depth	25.491	mm
22	α_t	Tooth tip angle	31.699	○
23	w_{op}	Slot opening	2.935	mm
24	w_p	Barrier post	0.511	mm
25	e_c	End carrier	3.122	mm
26	ϑ_{min}	Min. angle	15.069	○
27	ϑ_{max}	Max. angle	42.383	○
28	r_f	Fillet radius	0.240	mm

Table 3. Complete list of optimization parameters.

No:	Symbol	Description	Boundaries	Unit
29	$\Delta r_{1\text{ in}}$	Barrier offset	[0 1]	mm
30	$\Delta r_{1\text{ out}}$	Barrier offset	[0 1]	mm
31	$\Delta r_{2\text{ in}}$	Barrier offset	[0 1]	mm
32	$\Delta r_{2\text{ out}}$	Barrier offset	[0 1]	mm
33	$\Delta r_{3\text{ in}}$	Barrier offset	[0 1]	mm
34	$\Delta r_{3\text{ out}}$	Barrier offset	[0 1]	mm
35	$\Delta r_{4\text{ out}}$	Barrier offset	[0 1]	mm

3. Automated Geometry Construction

Any optimization requires automatic design generation. As mentioned earlier, a higher number of optimization variables is associated with a longer optimization time. Gamba et al. [30] have shown that three variables per barrier ($3 \cdot k$, where k is the number of barriers) is the appropriate number of parameters to use for a fast yet accurate description of multi-barrier SyRM. To reduce this even further, the $2 + (2 \cdot k - 1)$ alternative is proposed in this paper. Several rotor barrier types are commonly used in SyRM design: circular, hyperbolic, fluid (Zhukovsky), segmented, etc. (open-source SyRE project offers more details and instructions on geometry generation [31]).

Within this paper, barrier line profiles (Figure 2) are derived from conformal mapping theory and the Zhukovsky airflow potential formulation [30,31]. This was originally developed to describe the flow paths of fluids channeled by two infinite plates forming an

angle π/p, and a plug centered at the origin of the reference frame (p is the number of pole pairs). In the solid rotor context, the plug represents the non-magnetic shaft with a radius of $D_{sh}/2$. Equations (1) and (2) express the magnetic field potential lines in parametric form.

$$C(\vartheta, r, \Delta r) = \sin(p\vartheta)\frac{\left(\frac{r+\Delta r}{D_{\text{sh}}/2}\right)^{2p} - 1}{\left(\frac{r+\Delta r}{D_{\text{sh}}/2}\right)^{p}}, \tag{1}$$

$$r(\vartheta, C) = \frac{D_{\text{sh}}}{2}\sqrt[p]{\frac{C + \sqrt{C^2 + 4\sin^2(p\vartheta)}}{2\sin(p\vartheta)}}; 0 \geq \vartheta \geq \pi/p. \tag{2}$$

3.1. Single Barrier Construction

The first step in creating the flux barrier is to select the point E_k in polar coordinates. E_k consists of two components, the radial component $r_k = (D_b - 2\delta)/2 - w_{\text{bb}}$, which has a fixed value, and the variable angle ϑ_k (5). The centerline parameter C_k is computed by solving the Equation (6). Virtual center barrier line is then computed by solving Equation (7). It is important to note that the angle vector should be generated in the range $\vartheta \in \left[\vartheta_k - \frac{\pi}{2p}, \vartheta_k\right]$; otherwise, if the angle is close to $\frac{\pi}{2p}$, the radial component will be weighted to infinity, leading to a computational error. The point G_k (8) is the center barrier coordinate (always lies at angle $\frac{\pi}{2p}$) and a reference point for calculating the inner and outer barrier line.

The barrier is constructed from a virtual centerline, which is modified by adding offsets Δr_{in} and Δr_{out} to form inner and outer flux lines (Figure 3). Offsets in millimeters are calculated from per-unitized input offset parameters according to expressions (4), (3), where $d_{k_{\text{in}}}$ and $d_{k_{\text{out}}}$ represent distance between G_k points according to Figure 4.

$$\overbrace{\Delta r_{k_{\text{out}}}}^{[\text{mm}]} = \overbrace{\Delta r'_{k_{\text{out}}}}^{\text{Per unit} \in [0 \quad 1]} \cdot d_{k_{\text{out}}}, \tag{3}$$

$$\overbrace{\Delta r_{k_{\text{in}}}}^{[\text{mm}]} = \overbrace{\Delta r'_{k_{\text{in}}}}^{\text{Per unit} \in [0 \quad 1]} \cdot d_{k_{\text{in}}}, \tag{4}$$

$$E_k = r_k \angle \vartheta_k, \tag{5}$$

$$C_k(\vartheta_k, r_k, \Delta r = 0), \tag{6}$$

$$r_k\left(\vartheta \in \left[\vartheta_k - \frac{\pi}{2p}, \vartheta_k\right], C_k\right), \tag{7}$$

$$G_k = r\left(\frac{\pi}{2p}, C_k\right) \angle \frac{\pi}{2p}. \tag{8}$$

The next step in the construction of the barrier is to compute $C_{k_{\text{out}}}$ (9) and $C_{k_{\text{in}}}$ (11), which completely define the equations of the inner and outer barriers. Solving the Equation (2) $= r_k$ with the arguments $C_{k_{\text{in}}}, C_{k_{\text{out}}}$ gives the intersection point angles $\vartheta_{k_{\text{in}}}, \vartheta_{k_{\text{out}}}$. The last step is the calculation of barrier lines r_{out} (10) and r_{in} (12) over the given angles.

$$C_{k_{\text{out}}}\left(\frac{\pi}{2p}, r_{G_k}, \Delta r_{k_{\text{out}}}\right), \tag{9}$$

$$r_{\text{out}}\left(\vartheta \in \left[\vartheta_{k_{\text{out}}} - \frac{\pi}{2p}, \vartheta_{k_{\text{out}}}\right], C_{k_{\text{out}}}\right), \tag{10}$$

$$C_{k_{\text{in}}}\left(\frac{\pi}{2p}, r_{G_k}, -\Delta r_{k_{\text{in}}}\right), \tag{11}$$

$$r_{\text{in}}\left(\vartheta \in \left[\vartheta_{k_{\text{in}}} - \frac{\pi}{2p}, \vartheta_{k_{\text{in}}}\right], C_{k_{in}}\right). \tag{12}$$

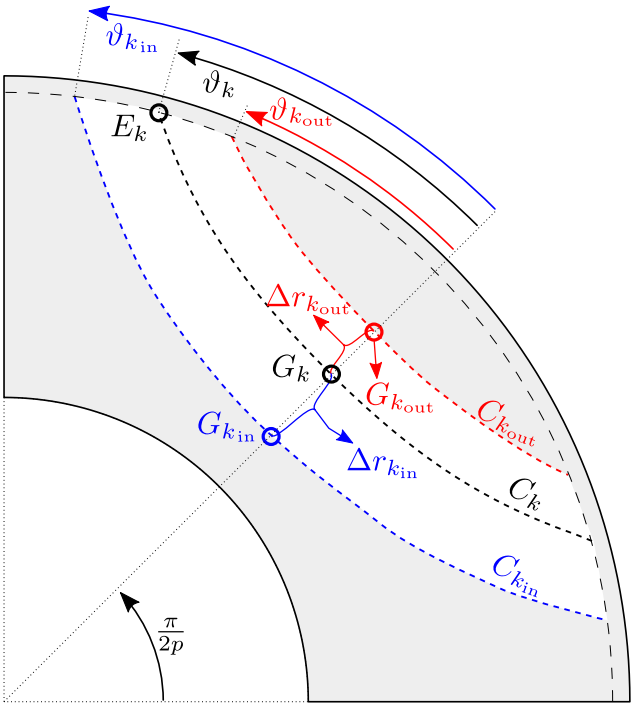

Figure 3. Construction of single barrier.

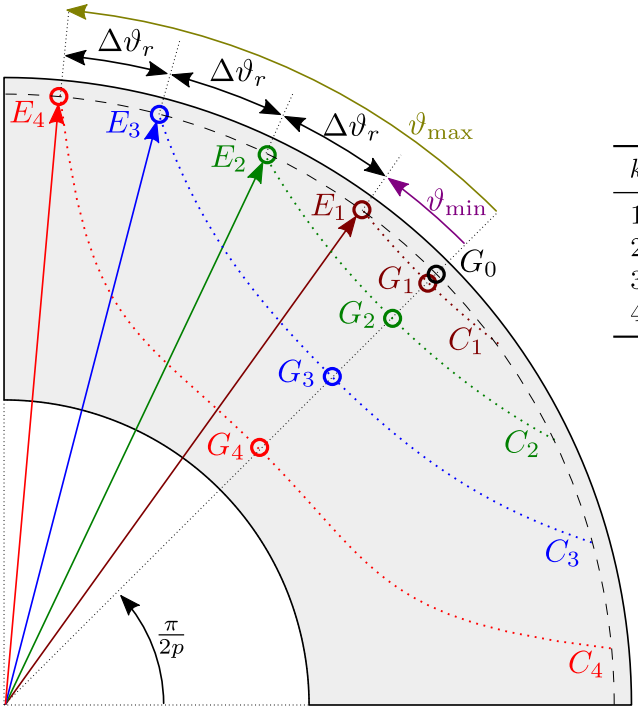

k	$\boldsymbol{d_{k_{\text{in}}}}$	$\boldsymbol{d_{k_{\text{out}}}}$
1	$d_{G_{12}}$	$d_{G_{10}}$
2	$d_{G_{23}}$	$d_{G_{21}}$
3	$d_{G_{34}}$	$d_{G_{32}}$
4	0	$d_{G_{43}}$

Figure 4. Construction of all flux barriers.

3.2. Construction of All Rotor Flux Barriers

The previous section described the flux barrier construction based on three parameters: variable angle ϑ_k, inner (Δr_{in}) and outer (Δr_{out}) barrier offsets. If all barriers were constructed according to this principle, the total parameter number would be $3 \cdot k$. Considering that center virtual barrier line is not part of the final barrier, there is a way to reduce the total number of parameters. Two angles, ϑ_{min} and ϑ_{max}, indicate the allowed center barrier line range. Depending on the number of barriers k, they define angles $\vartheta_{1..k}$ with equidistant angular offsets $\Delta\vartheta_r$ defining points $E_{1..k}$ used to construct each virtual center barrier line (Figure 4). To make the procedure robust, and to avoid clashes with the shaft, final barrier

(closest to the shaft) inner offset value is always zero. This procedure reduces the total number of barrier parameters to $2 + (2 \cdot k - 1)$. The constant 2 refers to the parameters $\vartheta_{\min}$ and $\vartheta_{\max}$, -1 refers to the constant $\Delta r_{\text{final in}} = 0$, which can be removed from the total number of parameters.

The choice of equidistant virtual flux line angle offset $(\Delta\vartheta_r)$ might appear to be a design-limiting constraint, but this is not the case. The virtual lines are used only as a reference for calculating the inner and outer barriers. Only in the special case, they represent flux barrier middle line when $\forall\Delta r_{k_{\text{out}}} = \forall\Delta r_{k_{\text{in}}}$. Optimization results proved that $\forall\Delta r_{k_{\text{out}}} \neq \forall\Delta r_{k_{\text{in}}}$ (Table 4). Furthermore, $\forall\Delta r_{k_{\text{out}}} \neq 0$ and $\forall\Delta r_{k_{\text{in}}} \neq 0$ (except in the final barrier, where $\Delta r_{\text{final in}} = 0$ by default). This proves that the assumption of equidistant virtual line offset angles has no effect on the final rotor design and can be used in the case of the Zhukovsky flux barrier type.

Table 4. Optimized rotor parameters and final result comparison.

		Random Generated						**Forced Feasibility**						
Result	**Unit**	**89**	**91**	**106**	**132**	**160**	**AVG**	**77**	**87**	**88**	**94**	**132**	**AVG**	
$\Delta r_{1\text{ in}}$	mm	2.26	1.29	1.64	1.87	2.51	1.91	2.53	2.58	2.75	1.26	2.76	2.37	
$\Delta r_{1\text{ out}}$	mm	0.46	1.00	1.24	0.87	0.37	0.79	0.54	0.39	0.03	0.79	0.42	0.43	
$\Delta r_{2\text{ in}}$	mm	2.06	2.13	1.77	1.70	1.00	1.73	1.40	1.30	0.81	1.03	2.12	1.33	
$\Delta r_{2\text{ out}}$	mm	1.18	1.80	1.70	1.36	1.46	1.50	1.05	1.36	1.73	2.50	0.56	1.44	
$\Delta r_{3\text{ in}}$	mm	2.91	2.11	2.69	2.15	3.07	2.59	2.98	1.76	1.99	2.36	1.29	2.08	
$\Delta r_{3\text{ out}}$	mm	1.45	1.71	1.24	1.87	2.06	1.67	1.85	1.95	2.19	2.10	2.30	2.08	
$\Delta r_{4\text{ out}}$	mm	3.73	4.52	4.26	4.58	3.41	4.10	3.64	4.71	4.41	4.23	4.65	4.33	**Diff. [%]**
η	-	0.91	0.91	0.91	0.91	0.91	0.91	0.91	0.91	0.91	0.91	0.91	0.91	0.00
$T_{\text{trans,skew}}$	Nm	603.7	602.9	603.3	603.6	603.2	603.3	604.1	605.2	604.5	604.0	604.9	604.5	0.20
$B_{\text{sy,max}}$	T	1.60	1.60	1.60	1.60	1.59	1.60	1.60	1.60	1.60	1.60	1.60	1.60	0.00
$B_{\text{st,max}}$	T	1.79	1.79	1.80	1.79	1.79	1.79	1.79	1.79	1.79	1.79	1.80	1.79	0.00
$\cos\varphi$	-	0.66	0.66	0.66	0.66	0.66	0.66	0.66	0.66	0.66	0.66	0.66	0.66	0.00
T_{ripple}	%	2.65	3.25	1.64	1.72	3.46	2.54	2.88	2.86	2.41	1.93	2.89	2.59	1.95

4. Optimization Procedure Details

The optimization of the 2D cross-section is set up as a single-objective problem mathematically defined as: Find the vector of parameters (13), subject to D parameter boundary constraints (14) and subject to m inequality constraint functions (15), which will maximize objective function (16).

$$\vec{x} = [x_1, x_2, \ldots, x_D], \quad \vec{x} \in R^D, \tag{13}$$

$$x_i^{(L)} \leq x_i \leq x_i^{(U)}, \quad i = 1, \ldots, D \tag{14}$$

$$g_j(\vec{x}) \leq 0, \quad j = 1, \ldots, m, \tag{15}$$

$$max\, f(\vec{x}). \tag{16}$$

The applied optimization workflow is shown in Figure 5. The optimization process starts with the problem definition (boundaries, constraints, objectives, etc.) and a preset of constant parameters (slots, poles, active diameter, etc.).

After entering the optimization loop, the following steps are performed iteratively:

1. the optimization algorithm generates the vector $\vec{x}$ (optimization variables);
2. variables are converted to model parameters;
3. model is generated based on the model parameters;
4. model is solved;
5. performance is extracted from the solution (values for constraints and objective functions are calculated from the solution);
6. data is passed to the optimization algorithm.

Single-objective optimization has only one objective function, which may have multiple variables and scaling factors. When the optimization converges, the value of the objective function saturates around a certain value. Without stopping criteria, the objective function will improve in infinitesimal steps for a very long time without any significant design improvement. In this paper, the following stopping criteria are used: after each generation, the last four objective function increments $f_{1..4}$ are checked; if the difference between f_1 and f_4 is less than 0.2%, the optimization is stopped; otherwise, it continues until the 160th generation.

5. Model and Solution Feasibility

In optimization problems, the notion of feasibility is related to the acceptance criteria of the solution. A solution is declared feasible if it satisfies certain criteria (15). The feasibility of a solution implies that a solution exists, i.e., the problem or model that provides this solution is solvable. During the optimization process, models may occur that are not solvable. These models have no solution and can be declared infeasible without solving them, which can decrease computational burden in the case of FEA-based solver. The models that are not solvable are declared as infeasible considering the model feasibility criteria.

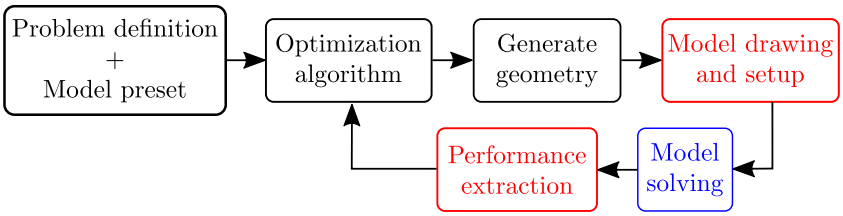

Figure 5. Optimization workflow.

5.1. Geometrical Feasibility

A special subset of model feasibility criteria is geometric feasibility, which characterizes whether the model geometry satisfies certain criteria (e.g., mechanical integrity, physicality, overlaps, etc.). In some cases, trying to solve a geometrically infeasible model with external solvers can lead to a crash of the whole optimization routine, a problem that highlights the need for detection methods to deal with geometrically infeasible models (e.g., barrier 1 (blue) collides with barrier 2 (yellow), the overlap is marked in red, Figure 6c).

To avoid the construction of such an invalid model, a geometric feasibility procedure can be performed within the optimization algorithm for each candidate vector. Regardless of the method of handling and detecting geometric infeasibility, it is always beneficial to reduce the occurrence of infeasible models. The simplest method for reducing the occurrence of geometrically infeasible models is to introduce lower and upper parameter bounds, which can be in the form of linear (Figure 7a), non-linear function bounds (Figure 7b), or complex bounds (Figure 7c).

For simple problems, the introduction of bounds can completely avoid the occurrence of infeasible models, while for complex problems it reduces the probability of the occurrence of the infeasible candidates. For this reason, optimization algorithms must include a method for dealing with geometrically infeasible candidates.

In general, a geometrically infeasible candidate is discarded while the new candidate takes its place. To generate a replacement candidate, Žarko et al. [25,32] randomly initialize the entire parameter set (13) until a geometrically feasible replacement candidate appears. The drawback of this method is a possible rejection of candidates with some good properties. Moreover, this method may lead to slow convergence to the optimal solution if the optimal candidate is on the boundary of the feasible space.

The alternative approach is forced feasibility, where each infeasible design is subjected to parameter modification until feasibility is achieved (i.e., barrier 1 (blue) and barrier 2 (yellow) are modified until the candidate achieves the specified flux carrier width w_{goal}, Figure 6d). This approach requires smart parametrization with minimum feasibility con-

straints and can potentially be extremely complex. On the other hand, potential benefits include reduced optimization time (no need to wait for a random feasible design to emerge) and faster convergence to the final result. The substitution of infeasible candidates is implemented in the form of a projection onto the feasible space (Figure 7d).

Projection operator can be mathematically written as:

$$P = min[(\vec{x}_{\text{orig}} - \vec{x}_{\text{new}}) \cdot Q(\vec{x}_{\text{orig}} - \vec{x}_{\text{new}})^T], \tag{17}$$

$$Q = \begin{bmatrix} q_1 & 0 & \cdots & 0 \\ 0 & q_2 & \cdots & 0 \\ \vdots & \vdots & \ddots & \vdots \\ 0 & 0 & \cdots & q_D \end{bmatrix}, \tag{18}$$

$$\forall \vec{x}_{\text{new}} \in R^D$$

where $\vec{x}_{\text{orig}}$ represents parameter vector of original, geometrically infeasible candidate, $\vec{x}_{\text{new}}$ is its geometrically feasible replacement/alternative, and Q is weighting matrix (18) in which its coefficients control the projection path (1, 2, and 3 in Figure 7d). If all coefficients satisfy $q_{1..D} = 1$, projection is orthogonal, and the new geometrically feasible candidate is closest to the original infeasible candidate.

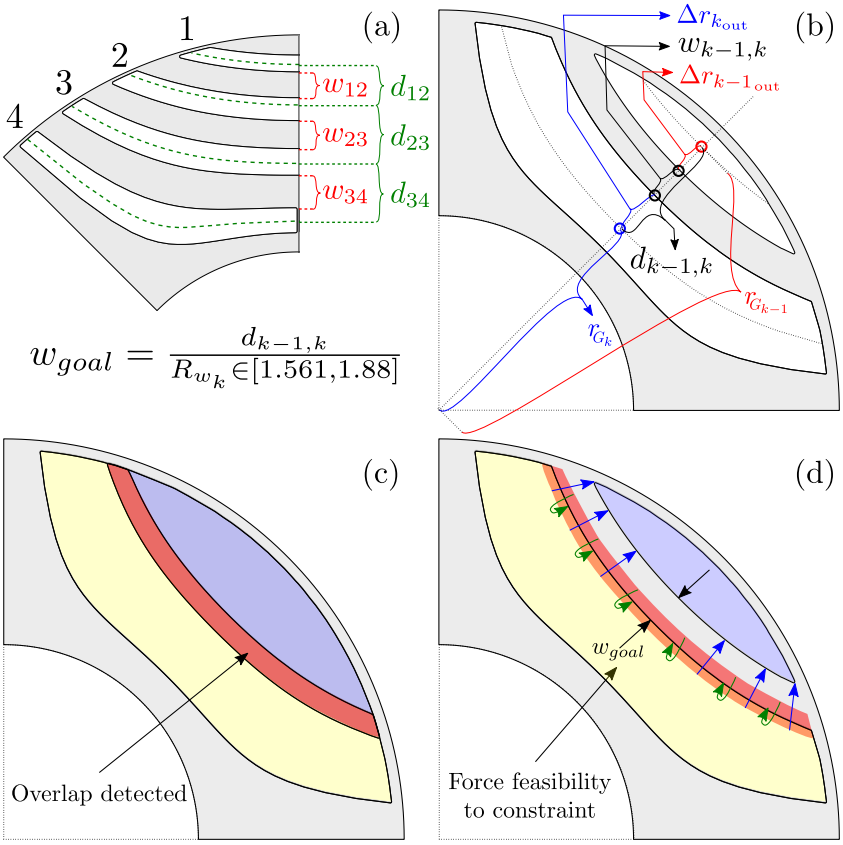

Figure 6. Empirical flux carrier width range (**a**); feasibility check parameters (**b**); infeasible geometry (**c**) and forced feasibility (**d**).

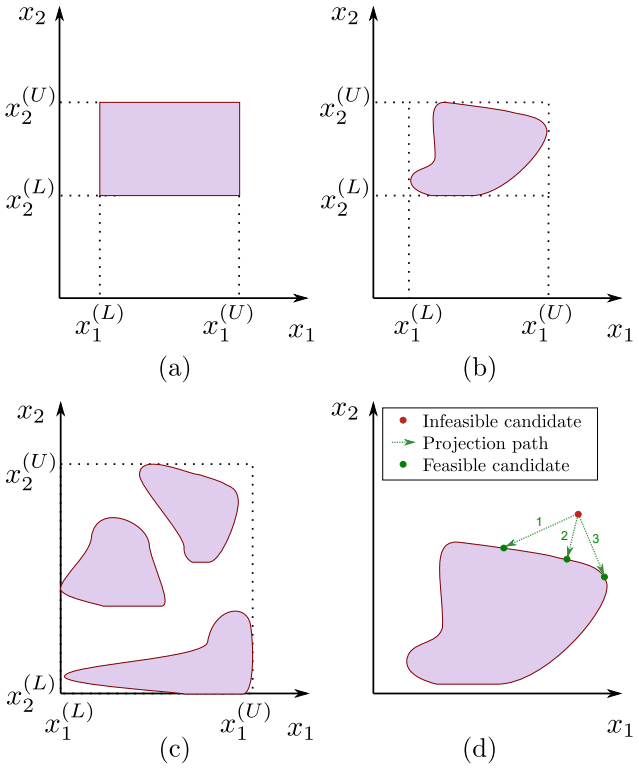

Figure 7. Optimization function bounds: (**a**) simple, (**b**) non-linear, and (**c**) complex. Candidate projection on feasible space (**d**).

5.2. Forced Feasibility Algorithm

For simplicity, the functionality is explained using two barrier SyRM (Figure 6b–d). The first step is geometry generation based on the parameterization approach from Section 3 (Algorithm 1: ln: 1–5). The next step is to compute the variables $d_{k-1,k}$, $w_{k-1,k}$, w_{goal} (Figure 6b) and check whether the infeasibility condition is satisfied (Algorithm 1: ln: 11). The design may be infeasible for one of two reasons: there is a barrier conflict ($w_{k-1,k} \leq 0$) or the flux carrier width is too small ($w_{k-1,k} \leq w_{\text{goal}}$). If not feasible (Figure 6c), proceed to forcing feasibility (Algorithm 2).

The purpose of the force feasibility function (Algorithm 2: ln: 1) is to provide the current position information of the barrier (w_{goal}, $d_{k-1,k}$, $\Delta r_{k_{out}}$, $\Delta r_{k-1_{in}}$, Figure 6b) and provide minimally modified barrier offsets ($\Delta r'_{k_{out}}$, $\Delta r'_{k-1_{in}}$), defining a new feasible design (Figure 6d). The minimal deviation is secured via MATLAB function FMINCON function [33]. FMINCON default input parameters are listed in Algorithm 2: ln: 2–7, where x_c represents the current barrier offset vector.

During the search, FMINCON iteratively calls COSTFCN, which is responsible for the convergence of the search (calculates the deviation of the generated x and the initial offset vector x_c), and CONSTRAINTFCN which calculates the deviation of the generated flux carrier width (w) from the carrier width (w_{goal}). When the algorithm converges, FMINCON returns $\Delta r'_{k_{out}}$, $\Delta r'_{k-1_{in}}$, and a new feasible geometry is generated (Figure 6d).

In summary, when the system detects an infeasible case, such as in the example shown in Figure 6b, where 1st and 2nd barriers overlap, $\Delta r_{2\text{out}}$ and $\Delta r_{1\text{in}}$ are iteratively modified until flux carrier width w_{goal} is reached (Figure 6d). This prevents the generation of too thin or too wide barrier geometries and improves the optimization procedure. The flux carrier width is randomly generated according to the equation $w_{\text{goal}} = d_{k-1,k}/R_{w_k}$ in the range $R_{w_k} = [1.561, 1.88]$ (Figure 6a). The range is empirically derived from several optimized designs.

Algorithm 1 Check feasibility function

Get:
$r_{G_{1..k}}$ ▷ Virtual barrier mid points
$\Delta r_{1..k_{out}}$ ▷ Barrier outer offsets
$\Delta r_{1..k_{in}}$ ▷ Barrier inner offsets
$R_{w_{1..k}} \rightarrow Rnd([1.561, 1.88])$ ▷ Flux carrier width goal ratios
function CHECKFEASIBILITY
  for k=2:$N_{barriers}$ **do**
  ▷ Calculate distance between virtual barrier mid points
    $d_{k-1,k} = r_{G_{k-1}} - r_{G_k}$
    ▷ Calculate flux carrier width
    $w_{k-1,k} = (r_{G_{k-1}} - \Delta r_{k-1_{in}}) - (r_{G_k} + \Delta r_{k_{out}})$
    ▷ Calculate minimal flux carrier width
    $w_{\text{goal}} = d_{k-1,k} / R_{w_k}$
    if $w_{k-1,k} \leq 0$ or $w_{k-1,k} \leq w_{\text{goal}}$ **then**
    ▷ Barriers are not feasible, force feasibility
      function FORCEFEASIBILITY($w_{\text{goal}}, d_{k-1,k}, \Delta r_{k_{out}}, \Delta r_{k-1_{in}}$)
        ...
      return $\Delta r'_{k_{out}}, \Delta r'_{k-1_{in}}$

Algorithm 2 Force feasibility function

function FORCEFEASIBILITY
  $A, B, A_{eq}, B_{eq} = [\,]$ ▷ empty FMINCON parametes
  $opt \rightarrow$ default ▷ Use default FMINCON options
  $lb = [0 \quad 0]$ ▷ Lower minimization bounds
  $ub = [d_{k-1,k} \quad d_{k-1,k}]$ ▷ Uppper minimization bounds
  $x_0 = 0.5 \cdot ub$ ▷ Initial guess
  $x_c = [\Delta r_{k_{out}} \quad \Delta r_{k-1_{in}}]$ ▷ Minimization goal

  ▷ Find a solution which satisfies constraints and minimally changes input parameters x_c via FMINCON function

  function FMINCON(COSTFCN, $x_0, B, A_{eq}, B_{eq}, lb, ub$,CONSTRAINTFCN, $w_{\text{goal}}, d_{k-1,k}, x_c$, opt, k)

  ▷ FMINCON iteratively calls COSTFCN, CONSTRAINTFCN and returns values which satisfy the constraint(s) with minimal deviation from current offset vector x_c
    ...
  return $\Delta r'_{k_{out}}, \Delta r'_{k-1_{in}}$

  function COSTFCN(x, x_c, k)
  ▷ COSTTFCN is responsible for result search convergence
    $f = (x - x_c).^2$
    $F = Sum(f)$
  return F

  function CONSTRAINTFCN($x, w_{\text{goal}}, d_{k-1,k}$)
  ▷ CONSTRAINTFCN calculates the deviation of generated flux carrier width from the goal width
    $x(1) \rightarrow \Delta r_{k_{out}}$
    $x(2) \rightarrow \Delta r_{k-1_{in}}$
    $w = \left(r_{G_{k-1}} + x(2)\right) - \left(r_{G_k} + x(1)\right)$
      $= d_{k-1,k} - x(1) - x(2)$
    $P = w_{\text{goal}} - w$
  return P

return $\Delta r'_{k_{out}}, \Delta r'_{k-1_{in}}$

Overall, this system does not discard randomly generated infeasible geometry, but modifies it until feasibility is achieved (hence the name "forced" feasibility). A similar procedure can be implemented for any problem that can be described by smooth analytic functions implemented as user-defined CONSTRAINTFCN.

5.3. Handling of Inequality Constraints

Inequality constraints usually arise from various electromagnetic, thermal, mechanical, manufacturing, economic, or normative limits, such as maximum flux density in the stator tooth, maximum magnet temperature, maximum stress in the rotor bridge, minimum magnet dimensions, maximum active material cost, maximum noise, etc. [32].

The traditional approach to constraint handling uses penalty functions to penalize the solutions that violate the constraints. This principle is implemented in terms of weighted sums that modify each objective function. Despite the popularity of penalty functions, they have several drawbacks. The most important is the need for careful fine-tuning of the penalty factors responsible for efficiently approximating the feasible range. Moreover, this method may suffer from problems related to poor choice of weighting factors, which may affect convergence. In this paper, we use an improved constraint function algorithm developed by Žarko et al. [34].

Inequality constraints for this particular case are defined in Table 5. The constraint function g_1 checks rotor structural factor of safety at maximum over-speed ($1.2 \cdot n_{\max}$).

Table 5. List of inequality constraints.

No:	Constraint Description	Symbol	Limit
g_1	Stress yield factor at $1.2 \cdot n_{\max}$	$\mathrm{FOS}_{\min}$	$\geq$2
g_2	Magnetostatic torque at n_b	T_{static}	$\geq$600 Nm
g_3	Flux density in stator yoke	$B_{\mathrm{sy,max}}$	$\leq$1.6 T
g_4	Flux density in stator tooth	$B_{\mathrm{st,max}}$	$\leq$1.8 T
g_5	Power factor	$\cos\varphi_{\min}$	$>$0.6
g_6	Torque ripple with skewing	$T_{\mathrm{ripple,max}}$	$\leq$10 %

The procedure related to constraint function g_2 contains several subfunctions designed according to ultra-fast scaling laws [29]. Multiple magnetostatic FEA calculations are performed to find the maximum torque versus current phase advance curve and to determine the optimal maximum torque-per-ampere (MTPA) control angle by polynomial fitting (the input machine has one turn per coil and one parallel path). The number of turns per coil and the number parallel paths of the machine is then matched to the required base speed. The optimization initially assumes a fixed stack length (Table 2, parameter $l_{\mathrm{s\,max}}$). If the calculated torque at $l_{\mathrm{s\,max}}$ is smaller than required, the machine design does not satisfy the constraint. Finally, it is checked whether the stator phase current is smaller than the maximum inverter current; otherwise, the constraint is not satisfied. After this step, all magnetostatic calculations are completed. The results are extracted and evaluated in the following constraint functions. Constraint g_3 checks the maximum stator yoke flux density, while g_4 checks the maximum tooth flux density. The purpose is to penalize the high saturation and the designs with increased iron losses.

Finally, a transient FEA calculation is performed at base speed to determine the power factor, average torque, torque ripple, and terminal voltage. Constraint g_5 checks the power factor. The primary goal in this ePTO optimization case study was maximization of the average torque, while torque ripple was of secondary importance, therefore being handled in the constraint (g_6). As a torque-ripple mitigation option, a rotor skew was selected. Skewing angle is one stator slot or $360^\circ/36 = 10^\circ$ mechanical degrees [35]. Without loss of generality, other more affordable, or more practical, torque-ripple mitigation techniques can be applied to this problem [36,37]. In addition, torque ripple can be included as another

optimization objective so that the design trade-off is made on the Pareto front of torque versus torque ripple.

If all constraints are satisfied, the final step is to compute the objective function f (19). η is the efficiency, and $T_{\text{trans,skew}}$ is the transient torque with applied rotor skew. The constants 700 and 0.96 represent scaling coefficients, which are used for combining torque and efficiency within a single objective function. Furthermore, these values are important for proper optimization convergence and were intentionally chosen to be larger than the peak torque and efficiency at the base speed to constrain the objective function to values ≤ 2 (important for the final comparison of the optimization convergence of forced feasibility and randomly generated geometries).

$$f = \frac{T_{\text{trans,skew}}}{700} + \frac{\eta}{0.96}. \tag{19}$$

6. Optimization Results

Five consecutive optimization runs of the DE algorithm with population size $\text{NP} = 24$ of geometries generated both randomly and with forced feasibility were performed (results in Tables 4 and 6).

To reduce optimization time and compare both approaches, most of the design parameters were taken from a previously optimized design [3]. Twenty-eight parameters were frozen (Table 2), and only 7 parameters were used for optimization (Table 3). This trade-off yields the same average objective function result (difference is +0.05%).

The average number of generations required to achieve convergence in the random generation case is 115.6, and 95.6 in the forced feasibility case, which is a reduction of 17.3%. In addition, in terms of computation time, the average convergence of forced feasibility is 3.34 h shorter (12.3% reduction).

When comparing the average torque results ($T_{\text{trans,skew}}$), both approaches yield practically the same outcome (Table 4). The remaining results (η, $B_{\text{sy,max}}$, $B_{\text{st,max}}$, $\cos\varphi$, T_{ripple}) are identical for forced feasibility and random generation. This is expected for two reasons: most of the parameters were taken from Reference [3], and the optimization algorithm is the same. Finally, the identical results confirm that forced feasibility does not affect negatively the optimization outcome.

Table 6. Optimization results.

Random Generated			**Forced Feasibility**		
Generation	f	**t [h]**	**Generation**	f	**t [h]**
89	1.8129	20.3	77	1.8136	18.9
91	1.8124	21.2	87	1.8145	21.2
106	1.8128	24.9	88	1.8132	21.9
132	1.8128	31.5	94	1.8133	23.8
160	1.8124	37.5	132	1.8133	32.9
Average			**Average**		
115.6	1.81266	27.08	95.6	1.81358	23.74

Table 4 summarizes the optimized rotor parameters for both optimization approaches. As mentioned earlier, the most important result is the fact that all parameters are greater than zero (neither the inner nor the outer blocking line sticks to the virtual centerline) and $\forall \Delta r_{k_{\text{out}}} \neq \forall \Delta r_{k_{\text{in}}}$. All optimized cross sections are shown in Figure 8, which confirms that the position of the centerline of the virtual barriers does not affect the optimization result.

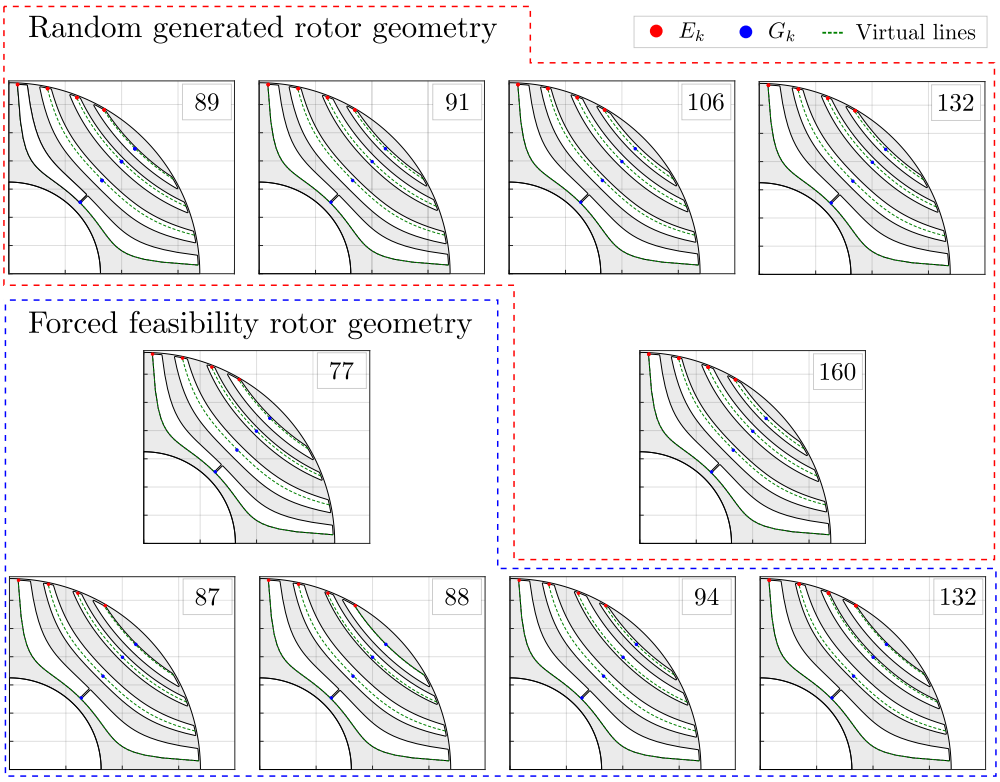

Figure 8. Comparison of optimized geometries in case of random generated and forced feasibility approach.

7. Conclusions

This paper demonstrates a novel automatic design procedure of SyRM rotor with minimum number of geometric parameters, which simplifies the design generation and reduces the optimization time. The presented procedure is implemented into an existing single objective DE optimization algorithm framework which interrupts evaluation of constraint functions when the inequality constraint is violated, thus saving computation time.

The second paper contribution is the introduction of novel forced feasibility concept which improves optimization convergence proved by successive comparative optimization runs with randomly generated rotor barrier geometries. The results show that properly implemented forced feasibility leads to a further reduction in optimization time (12.3% shorter).

The machine design originally presented in Reference [3] has 21 optimization variables. The entire optimization process took 7 days. Without the forced feasibility method, the process would be 12.3% longer (approximately 1 additional day). Considering that the optimization time is proportional to the number of parameters (i.e., a two- layer V-shape PM machine may have 44 parameters), it can be concluded that the total calculation time can be significantly reduced by using forced feasibility approach on different machine topologies.

Author Contributions: This paper is a continuation of the paper "Design and Optimization of Synchronous Reluctance Machine for actuation of Electric Multi-purpose Vehicle Power Take-Off" submitted for ICEM 2020 conference. B.B. created a preset model and automated geometry scripting with a minimal set of parameters. The original multi-objective optimization procedure was adapted to support single-objective optimization, which is easier to evaluate in terms of forced feasibility impact on optimization time reduction. B.B. adapted the original code developed by S.S., simulated the results, and prepared all tables and figures. S.S. supervised the process and formulated the contributions. T.J. worked on the mathematical formulation of the forced feasibility and the practical implementation of the algorithm through the MATLAB fmincon minimization function. All authors have read and agreed to the published version of the manuscript.

Funding: This work was partially supported by the Croatian Science Foundation under the project IP-2018-01-5822 - HYDREL.

Institutional Review Board Statement: Not applicable.

Informed Consent Statement: Not applicable.

Conflicts of Interest: The authors declare no conflict of interest.

Abbreviations

The following abbreviations are used in this manuscript:

EV	Electric vehicle
DE	Differential evolution
eMPV	Electric multipurpose vehicle
ePTO	Electric power take-off
FEA	Finite element analysis
IPM	Interior permanent magnet machine
MTPA	Maximum torque per ampere
PM	Permanent magnet
PTO	Power take-off
SyRM	Synchronous reluctance machine

References

1. European Environment Agency. Electric Vehicles in Europe. Available online: https://www.eea.europa.eu/publications/electric-vehicles-in-europe (accessed on 2 January 2012).
2. Ban, B.; Stipetić, S. Electric Multipurpose Vehicle Power Take-Off: Overview, Load Cycles and Actuation via Synchronous Reluctance Machine. In Proceedings of the 2019 International Aegean Conference on Electrical Machines and Power Electronics (ACEMP) & 2019 International Conference on Optimization of Electrical and Electronic Equipment (OPTIM), Istanbul, Turkey, 27–29 August 2019.
3. Ban, B.; Stipetic, S. Design and Optimization of Synchronous Reluctance Machine for actuation of Electric Multi-purpose Vehicle Power Take-Off. In Proceedings of the 2020 International Conference on Electrical Machines (ICEM 2020), Gothenburg, Sweden, 23–26 August 2020; p. 1.
4. Alberti, L.; Bianchi, N.; Boglietti, A.; Cavagnino, A. Core axial lengthening as effective solution to improve the induction motor efficiency classes. In Proceedings of the IEEE Energy Conversion Congress and Exposition: Energy Conversion Innovation for a Clean Energy Future (ECCE 2011), Phoenix, AZ, USA, 17–22 September 2011.
5. Bramerdorfer, G.; Cavagnino, A.; Vaschetto, S. Impact of IM pole count on material cost increase for achieving mandatory efficiency requirements. In Proceedings of the IECON (Industrial Electronics Conference), Florence, Italy, 24–27 October 2016.
6. Agamloh, E.B.; Boglietti, A.; Cavagnino, A. The incremental design efficiency improvement of commercially manufactured induction motors. *IEEE Trans. Ind. Appl.* **2013**, *49*, 2496–2504. [CrossRef]
7. El-Refaie, A.M. Motors/generators for traction/propulsion applications: A review. *IEEE Veh. Technol. Mag.* **2013**, *8*, 90–99.
8. Pellegrino, G.; Cupertino, F.; Gerada, C. Automatic Design of Synchronous Reluctance Motors Focusing on Barrier Shape Optimization. *IEEE Trans. Ind. Appl.* **2015**, *51*, 1465–1474. [CrossRef]
9. Lu, C.; Ferrari, S.; Pellegrino, G. Two Design Procedures for PM Synchronous Machines for Electric Powertrains. *IEEE Trans. Transp. Electrif.* **2017**, *3*, 98–107. [CrossRef]
10. Zhu, X.; Wu, W.; Quan, L.; Xiang, Z.; Gu, W. Design and Multi-Objective Stratified Optimization of a Less-rare-earth Hybrid Permanent Magnets Motor with High Torque Density and Low Cost. *IEEE Trans. Energy Convers.* **2018**, *34*, 1178–1189. [CrossRef]
11. Bonthu, S.S.R.; Choi, S.; Baek, J. Design Optimization with Multiphysics Analysis on External Rotor Permanent Magnet-Assisted Synchronous Reluctance Motors. *IEEE Trans. Energy Convers.* **2018**, *33*, 290–298. [CrossRef]
12. Tapia, J.A.; Parviainen, A.; Pyrhonen, J.; Lindh, P.; Wallace, R.R. Optimal design procedure for an external rotor permanent-magnet machine. In Proceedings of the 2012 20th International Conference on Electrical Machines (ICEM 2012), Marseille, France, 2–5 September 2012.
13. Lei, G.; Bramerdofer, G.; Ma, B.; Guo, Y.; Zhu, J. Robust Design Optimization of Electrical Machines: Multi-objective Approach. *IEEE Trans. Energy Convers.* **2020**, *36*, 390–401. [CrossRef]
14. Lei, G.; Bramerdorfer, G.; Liu, C.; Guo, Y.; Zhu, J. Robust Design Optimization of Electrical Machines: A Comparative Study and Space Reduction Strategy. *IEEE Trans. Energy Convers.* **2020**, *36*, 300–313. [CrossRef]
15. Babetto, C.; Bacco, G.; Bianchi, N. Synchronous Reluctance Machine Optimization for High-Speed Applications. *IEEE Trans. Energy Convers.* **2018**, *33*, 1266–1273. [CrossRef]
16. Xu, L.; Wu, W.; Zhao, W.; Liu, G.; Niu, S. Robust Design and Optimization for a Permanent Magnet Vernier Machine With Hybrid Stator. *IEEE Trans. Energy Convers.* **2020**, *35*, 2086–2094. [CrossRef]

17. Howard, E.; Kamper, M.J. Weighted Factor Multiobjective Design Optimization of a Reluctance Synchronous Machine. *IEEE Trans. Ind. Appl.* **2016**, *52*, 2269–2279. [CrossRef]
18. Kamper, M.J.; Van Der Merwe, F.S.; Williamson, S. Direct Finite Element Design Optimisation of the Cageless Reluctance Synchronous Machine. *IEEE Trans. Energy Convers.* **1996**, *11*, 547–553. [CrossRef]
19. Dmitrievskii, V.; Prakht, V.; Kazakbaev, V. IE5 Energy-Efficiency Class Synchronous Reluctance Motor with Fractional Slot Winding. *IEEE Trans. Ind. Appl.* **2019**, *55*, 4676–4684. [CrossRef]
20. Yamashita, Y.; Okamoto, Y. Design Optimization of Synchronous Reluctance Motor for Reducing Iron Loss and Improving Torque Characteristics Using Topology Optimization Based on the Level-Set Method. *IEEE Trans. Magn.* **2020**, *56*, 36–39. [CrossRef]
21. Storn, R.; Price, K. Differential Evolution—A Simple and Efficient Heuristic for Global Optimization over Continuous Spaces. *J. Glob. Optim.* **1997**, *11*, 341–359. [CrossRef]
22. Bramerdorfer, G.; Zavoianu, A.C.; Silber, S.; Lughofer, E.; Amrhein, W. Possibilities for Speeding Up the FE-Based Optimization of Electrical Machines-A Case Study. *IEEE Trans. Ind. Appl.* **2016**, *52*, 4668–4677. [CrossRef]
23. Liu, X.; Slemon, G.R. An improved method of optimization for electrical machines. *IEEE Trans. Energy Convers.* **1991**, *6*, 492–496. [CrossRef]
24. Stipetic, S.; Zarko, D.; Kovacic, M. Optimised design of permanent magnet assisted synchronous reluctance motor series using combined analytical-finite element analysis based approach. *IET Electr. Power Appl.* **2016**, *10*, 330–338. [CrossRef]
25. Zarko, D.; Stipetic, S.; Martinovic, M.; Kovacic, M.; Jercic, T.; Hanic, Z. Reduction of computational efforts in finite element-based permanent magnet traction motor optimization. *IEEE Trans. Ind. Electron.* **2017**, *65*, 1799–1807. [CrossRef]
26. Lampinen, J. Multi-Constrained Nonlinear Optimization by the Differential Evolution Algorithm. In *Soft Computing and Industry*; Springer: London, UK, 2002.
27. Price, K.; Storn, R. Matlab Code for Differential Evolution. Available online: http://www1.icsi.berkeley.edu/$\sim$storn/code.html (accessed on 23 January 2020).
28. Motor Design Ltd. Motor-CAD/Motor-LAB Software. Available online: https://www.motor-design.com/motor-cad/ (accessed on 23 January 2020).
29. Stipetic, S.; Zarko, D.; Popescu, M. Ultra-fast axial and radial scaling of synchronous permanent magnet machines. *IET Electr. Power Appl.* **2016**, *10*, 658–666. [CrossRef]
30. Gamba, M.; Pellegrino, G.; Cupertino, F. Optimal Number of Rotor Parameters for the Automatic Design of Synchronous Reluctance Machines. In Proceedings of the 2014 International Conference on Electrical Machines (ICEM 2014), Berlin, Germany, 2–5 September 2014; pp. 1334–1340.
31. Cupertino, F.; Pellegrino, G.; Cagnetta, P.; Ferrari, S.; Perta, M. SyRE: Synchronous Reluctance (Machines)—Evolution. Available online: https://sourceforge.net/projects/syr-e/ (accessed on 23 April 2021).
32. Stipetic, S.; Miebach, W.; Zarko, D. Optimization in design of electric machines: Methodology and workflow. In Proceedings of the Joint International Conference—ACEMP 2015: Aegean Conference on Electrical Machines and Power Electronics, OPTIM 2015: Optimization of Electrical and Electronic Equipment and ELECTROMOTION 2015: International Symposium on Advanced Electromechanical Moti, Side, Turkey, 2–4 September 2015; pp. 441–448.
33. Mathworks. Matlab Fmincon Function. Available online: https://se.mathworks.com/help/optim/ug/fmincon.html (accessed on 13 January 2020).
34. Žarko, D.; Stipetić, S. Criteria for optimal design of interior permanent magnet motor series. In Proceedings of the 2012 20th International Conference on Electrical Machines (ICEM 2012), Marseille, France, 2–5 September 2012.
35. Bomela, X.B.; Kamper, M.J. Effect of Stator Chording and Rotor Skewing on Performance of Reluctance Synchronous Machine. *IEEE Trans. Ind. Appl.* **2002**, *38*, 91–100. [CrossRef]
36. Ferrari, S.; Armando, E.; Pellegrino, G. Torque Ripple Minimization of PM-assisted Synchronous Reluctance Machines via Asymmetric Rotor Poles. In Proceedings of the 2019 IEEE Energy Conversion Congress and Exposition (ECCE), Baltimore, MD, USA, 29 September–3 October 2019; pp. 4895–4902.
37. Ferrari, S.; Pellegrino, G.; Davoli, M.; Bianchini, C. Reduction of Torque Ripple in Synchronous Reluctance Machines through Flux Barrier Shift. In Proceedings of the 2018 XIII International Conference on Electrical Machines (ICEM), Alexandroupoli, Greece, 3–6 September 2018; pp. 2290–2296.